Rhenium tetrazolato complexes coordinated to thioalkyl-functionalised phenanthroline ligands: synthesis, photophysical characterisation, and incubation in live HeLa cells

Melissa V. Werrett,[a] Phillip J. Wright,[a] Peter V. Simpson,[a] Paolo Raiteri,[a] Brian W. Skelton,[b] Stefano Stagni,[c] Alysia G. Buckley,[b] Paul J. Rigby,[b,*] Massimiliano Massi[a,*]

[a] *Nanochemistry Research Institute - Department of Chemistry, Curtin University, Kent St., 6102 Bentley WA, Australia.*

[b] *Centre for Microscopy, Characterisation and Analysis, University of Western Australia, Crawley, Perth, WA, 6009, Australia.*

[c] *Department of Industrial Chemistry "Toso Montanari", University of Bologna, viale del Risorgimento, Bologna 40126, Italy.*

Corresponding author email: paul.rigby@uwa.edu.au; m.massi@curtin.edu.au

Abstract

Three new complexes of formulation *fac*-[Re(CO)$_3$(**diim**)**L**], where **diim** is either 1,10-phenanthroline or 1,10-phenanthroline functionalised at position 5 by a thioalkyl chain, and **L** is either a chloro or aryltetrazolato ancillary ligand, were synthesised and photophysically characterised. The complexes exhibit phosphorescent emission with maxima around 600 nm, originating from triplet metal-to-ligand charge transfer states with partially mixed ligand-to-ligand charge transfer character. The emission is relatively long-lived, within the 200-400 ns range, and with quantum yields of 2-4%. The complexes were trialed as cellular markers in live HeLa cells, along with two previously reported rhenium tetrazolato complexes bound to unsubstituted 1,10-phenanthroline. All five complexes exhibit good cellular uptake and non-specific perinuclear localisation. Upon excitation at 405 nm, the emission from the rhenium complexes could be clearly distinguished from autofluorescence, as demonstrated by spectral detection within the live cells. Four of the complexes did not appear to be toxic, however prolonged excitation could result in membrane blebbing. No major sign of photobleaching was detected upon multiple imaging on the same cell sample.

Introduction

Luminescent heavy metal complexes have been proposed as an advantageous alternative to organic fluorophores for optical imaging. [1-4] Fluorescence from organic molecules is generally characterised by small Stokes shifts and short excited state lifetime (e.g. < 10 ns). These features might contribute to concentration quenching phenomena and the difficulty of discriminating between the fluorescence of the probe and endogenous autofluorescence. Furthermore, the tendency of organic fluorophores to photobleach often limits their use to rather short timeframes, thus hindering their application in extended live cell imaging. Transition metal complexes are in general triplet state emitters, hence their phosphorescence is characterised by longer Stokes shift values that aid in the prevention of concentration quenching. Moreover, longer excited state lifetimes are amenable to time-gated microscopies to eliminate background fluorescence.[5] Many of these metal complexes are also quite inert, both in the ground and excited state, making them resistant to photobleaching.[5] In addition, these metal complexes are able to efficiently sensitise the production of singlet oxygen ($^1O_2$), a highly toxic species for live cells. [6,7] Thus, particular care should be taken when using metal complexes to image live cells, due to the possible induction of toxic reactions. On the other hand, this feature is also appealing for the possible development of therapeutic strategies such as photodynamic therapy. [8,9] Therefore, photoactive metal complexes offer a potential platform for the development of theranostic agents. [10,11]

We have recently reported the photophysical investigation of the Re tetrazolato family of complexes, whose general formulation is *fac*-[Re(CO)$_3$(**diim**)**L**] with **diim** being either 1,10-phenanthroline (**phen**) or 2,2'-bipyridine and **L** an 5-aryltetrazolato ancillary ligand. [12,13] The study highlighted the fact that these complexes emit from their triplet metal-to-ligand charge transfer excited states (^{3}MLCT) mixed with triplet ligand-to-ligand excited states (^{3}LLCT). The emission is centred in the 580-610 nm region and can be significantly modulated by interaction of the tetrazole ring with electrophilic reagents, either reversibly (H^+)[14] or irreversibly (CH_3^+).[15] Functionalisation at the aryl ring proved to have almost negligible effect on the photophysical properties of the complexes. [12,13] This advantageous feature means that the biological properties of the complexes can be tuned by attachment of various functionalities at the aryl ring without perturbation of the spectral characteristics of the Re centres. In fact, optimisation of the photophysical and biological properties of luminescent transition metal complexes is often challenging, since they are in general both intimately linked to the chemical nature of the species.[16]

We have previously demonstrated how these complexes can efficiently act as cellular imaging agents. Our preliminary data in this area highlighted how different aryl groups bound to the tetrazole ring are able to modulate organelle specificity in live cells. Remarkably, the complex *fac*-

[$Re(CO)_3$(**diim**)**L**] with **L** being 5-(4-cyanophenyl)tetrazolate proved to be a unique complex able to stain the lipid droplets of live cells.[17]

With the idea of continuing our studies on the development of phosphorescent cellular markers based on Re tetrazolato complexes, we have turned our attention to the direct functionalisation of the **phen** ligand. For this purpose, we have chosen a thioalkyl chain at the position 5 of the diimine ligand. This small chain ending with an OH group can be further functionalised, and it was in this case appended with an ethylene glycol as a model group. This choice was inspired by the fact that polyethylene glycol moieties have proven to increase the biocompatibility of cellular markers and aid in cellular internalisation. [18,19] The three new complexes, for which a comprehensive photophysical study is here presented, are depicted in Figure 1 (**S-ReCl**, **EG-S-ReCl**, and **EG-S-ReTPh**). Their biological properties are investigated *via* incubation in live HeLa cells, and are also compared to two previously reported Re complexes (Figure 1; **ReTPh** and **ReTBz**).[12]

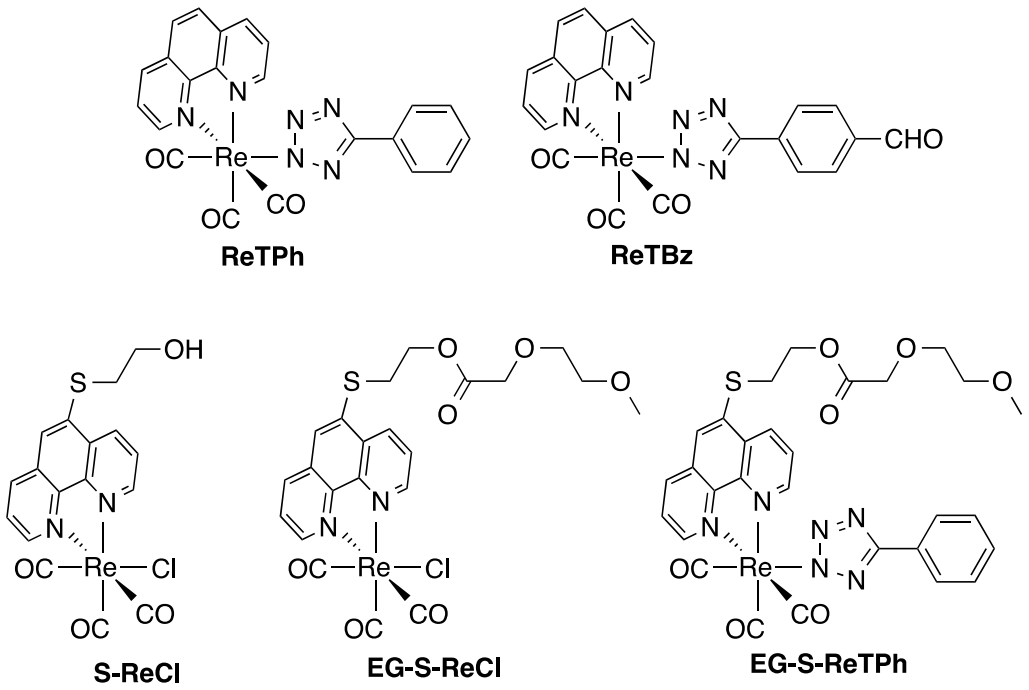

Figure 1. Rhenium complexes investigated in this work.

Results and Discussion

Synthesis and functionalisation of the complexes

The synthesis and characterisation of the complexes **ReTPh** and **ReTBz** is reported elsewhere.[12] To access the thioalkyl-functionalised complex **S-ReCl**, the previously reported *fac*-[$Re(CO)_3$(**ephen**)Cl],[20] where **ephen** is 5,6-epoxy-1,10-phenanthroline, was treated with 2-mercaptoethanol and sodium ethoxide in ethanol (Figure 2). The values of the stretching modes of the three carbonyl ligands (2016, 1907, and 1879 cm^{-1}) highlight the fact that the thioalkyl substituent of **phen** does not significantly alter the electron density on the Re centre. These values are very similar to those of the parent *fac*-[$Re(CO)_3$(**phen**)Cl] complex.[12]

Esterification of the OH group in **S-ReCl** was achieved using EDCI [1-ethyl-3-(3-dimethylaminopropyl)carbodiimide hydrochloride] and a catalytic amount of DMAP (4-dimethylaminopyridine), with **EG-S-ReCl** being isolated after column chromatography in a 31% yield (Figure 2). This methodology also allows the recovery of the starting **S-ReCl** complex, which can be conveniently recycled. Other attempts at obtaining **EG-S-ReCl** by reacting the acid chloride derived from 2-(2-methoxyethoxy)acetic acid with **S-ReCl** were unsuccessful, as was the use of DCC (dicyclohexylcarbodiimide) as the coupling agent with a catalytic amount of DMAP. In the latter case, analysis of the crude mixture revealed that the targeted **EG-S-ReCl** product was obtained in about 70% yield, but contaminated with dicyclohexylurea, and could not be purified by either recrystallisation or chromatography.

Treatment of **EG-S-ReCl** with silver triflate in $CHCl_3$ at reflux[21,22] and subsequent addition of 1H-5-phenyltetrazole and triethylamine[12] led to the formation of **EG-S-ReTPh** in a 17% yield. The stretching values of the carbonyl bands are found to increase in wavenumber to 2025 and 1908 cm^{-1} relative to **EG-S-ReCl**, with the two lower-energy peaks being quasi-degenerate and hence overlapped in a broad signal. These values are in agreement with a reduction in electron density on the Re centre, as expected upon exchanging the chloro with the π-acidic tetrazolato ligand. Furthermore, the chemical shift of the tetrazolic C atom at 163.7 ppm indicates the predominant coordination of the Re centre to the N2 atom of the tetrazolato ring. [12,13]

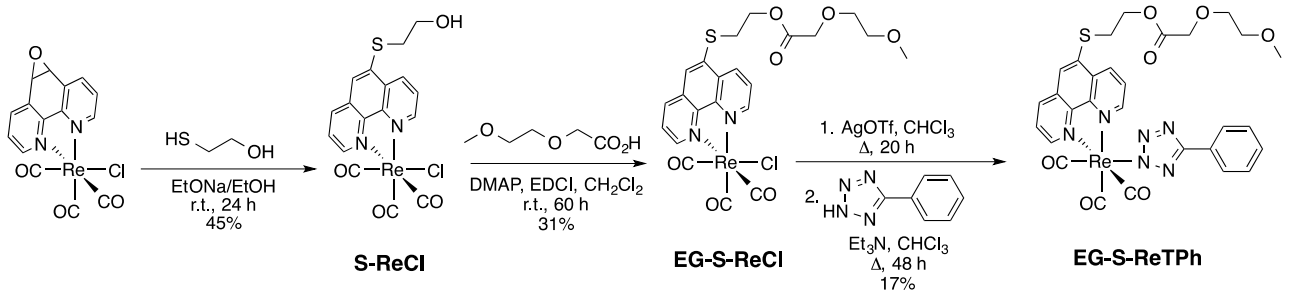

Figure 2. Synthesis of **S-ReCl**, **EG-S-ReCl** and **EG-S-ReTPh**.

X-ray structural characterisation

Single crystals suitable for X-ray diffraction were obtained for the complexes **S-ReCl** and **EG-S-ReCl**, projections of which are shown in Figure 3. The complexes are arranged in antiparallel pairs, where the terminal OH group from the thioalkyl chain of one complex engages in hydrogen bonding with the chloro ligand of the second complex. The paired complexes are related by a crystallographic inversion centre. Two unique complexes of **EG-S-ReCl** are included within the asymmetric unit, with differences being confined to minor conformational changes on the alkyl chains. The structures of both complexes highlight the expected *facial* arrangement of the three carbonyl ligands. Tables reporting selected bond lengths and angles can be found in the ESI.

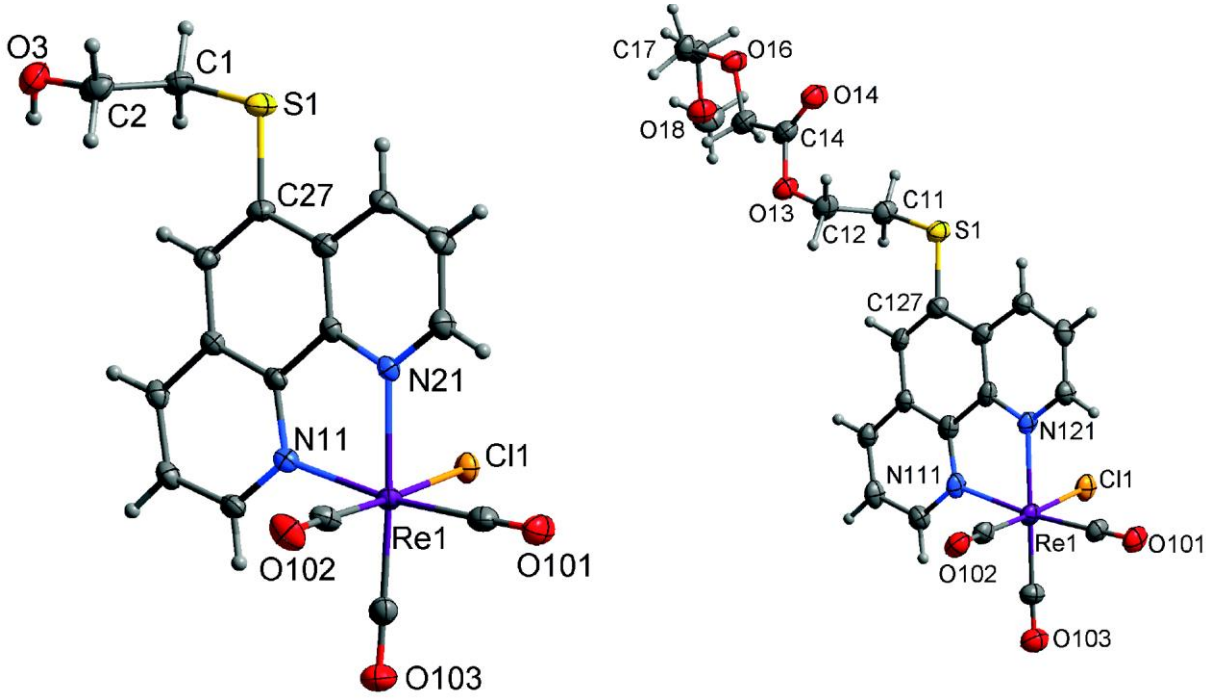

Figure 3. X-ray crystal structures of **S-ReCl** (left) and **EG-S-ReCl** (right). Atomic displacement ellipsoids have been drawn at the 50% probability level. Only one of the two individual complexes belonging to the asymmetric unit is reported for **EG-S-ReCl**. Lattice solvent molecules are omitted for clarity.

Photophysical investigation

Table 1. Summary of the photophysical data from diluted dichloromethane solutions at 298 and 77 K.

Complex	Absorption	Emission – 298 K							Emission – 77 K	
	λ_{abs} [nm] ($10^{-4}\varepsilon$ [$M^{-1}cm^{-1}$])	λ_{em} [nm]	τ [ns] aer	τ [ns] deaer	Φ aer	Φ deaer	k_r[a] [$10^5 s^{-1}$]	k_{nr}[b] [$10^6 s^{-1}$]	λ_{em} [nm]	τ [µs]
S-ReCl	245 (3.44)	626	128	210	0.018	0.020	0.952	4.667	520	198 (21%)
	300 (1.67)								562	688 (79%)
	348 (0.81)								610	
	416 (0.30)									
EG-S-ReCl	242 (3.51)	630	121	203	0.015	0.017	0.837	4.842	516	83 (18%)
	297 (1.77)								558	353 (82%)
	343 (0.84)								610	
	410 (0.39)									
EG-S-ReTPh	243 (8.28)	600	245	416	0.019	0.044	1.058	2.298	520	110 (12%)
	297 (3.86)								556	592 (88%)
	341 (1.96)								610	
	409 (0.36)									

[a] Calculated as [Φ/τ] using measurements from deaerated solutions; [b] calculated as [$(1-\Phi)/\tau$] using measurements from deaerated solutions.

The photophysical properties of **S-ReCl**, **EG-S-ReCl**, and **EG-S-ReTPh** were measured from diluted dichloromethane solutions (≈ 10^{-5} M) and are summarised in Table 1. The absorption spectra of the complexes are analogous (Figure 4). Intense transitions are present below 300 nm with values of molar absorptivity (ε) above 10^4 $M^{-1}cm^{-1}$. These bands are associated to ligand-centred (LC) $\pi\pi^*$ transitions occurring on the conjugated ligands **phen** and tetrazolato in the case of **EG-S-ReTPh**.[23] Two bands of lower intensity appear between 300 and 450 nm, which is generally the region associated to metal-to-ligand charge transfer transition (MLCT) mixed with ligand-to-ligand charge transfer transitions (LLCT).[23] To gain a better understanding on the nature of these two bands, the absorption spectra and the orbital contours were simulated with time-dependent density functional theory (TDDFT). The structures of the complexes were minimised using the implicit solvent model (PCM)[24] and resulted in good agreement with the structural data obtained via X-ray diffraction for **S-ReCl** and **EG-S-ReCl**, relative to the coordination sphere of the metal

centres. Differences in bond lengths were calculated within 0.02 and 0.06 Å, whereas differences in bond angles were calculated within 0.8 and 3.5°. An analysis of the TDDFT data (see ESI) reveals that the lower energy band with maximum at ≈ 410 nm originates from the HOMO-1 → LUMO transition for **S-ReCl** and **EG-S-ReCl** and HOMO → LUMO transition for **EG-S-ReTPh**. For each complex, the corresponding occupied orbital presents high metal character associated with ligand character (chloro or tetrazolato). On the other hand, the unoccupied orbital is localised on the **phen** ligand with no involvement of the thioalkyl functionalisation. Based on these data, the lower energy band is associated with the typical admixture of MLCT and LLCT. The higher energy band at ≈ 346 nm originates from the HOMO-2 → LUMO+1 transition for all the three complexes. Both of these orbitals are localised on the **phen** ligand and the HOMO-2 orbital contour highlights a significant contribution from the S atom. According to these data, the higher energy band is associated to an LC ππ* transition, with partial charge transfer character.

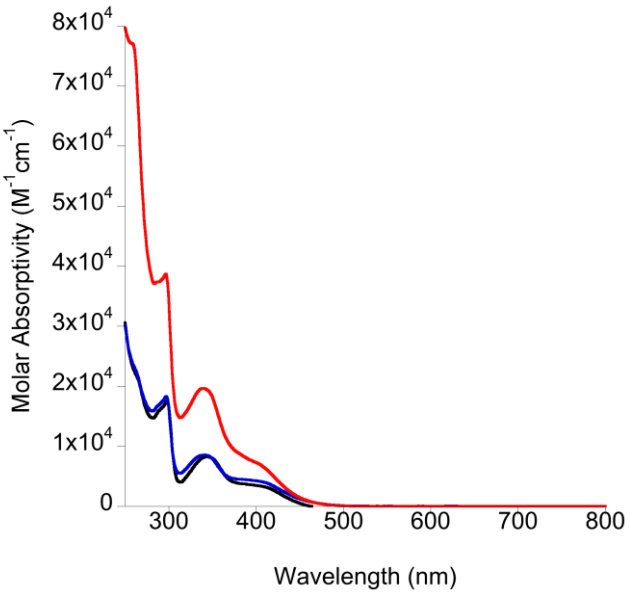

Figure 4. Absorption profiles for **S-ReCl** (black trace), **EG-S-ReCl** (blue trace) and **EG-S-ReTPh** (red trace) measured from diluted dichloromethane solutions at room temperature.

The emission profiles of the complexes, shown in Figure 5, exhibit broad and structureless bands, which are typical for admixtures of MLCT and LLCT transitions.[23] The emission maximum of **EG-S-ReTPh** is blue-shifted by ≈ 30 nm with respect to those of **S-ReCl** and **EG-S-ReCl**. In agreement with previously published Re tetrazolato complexes,[12] this shift can be explained by the reduction of electron density on the Re centre when the chloro ligand is substituted for the tetrazolato ligand. **EG-S-ReTPh** also possesses a slightly longer excited state lifetime τ and

quantum yield Φ, a trend that can be rationalised by considering the decrease in the non-radiative decay constant k_{nr} (Table 1), in agreement with the energy gap law.[25] The nature of the emissive state is described as a ^{3}MLCT partially mixed with ^{3}LLCT character. The triplet multiplicity is in agreement with the higher values of τ and Φ measured from deaerated solutions. Furthermore, all three complexes act as sensitisers for singlet oxygen, whose emission around 1275 nm originating from the $^1\Delta_g \rightarrow {}^3\Sigma_g^-$ radiative decay can be detected upon excitation of the complexes around 360 nm.[6]

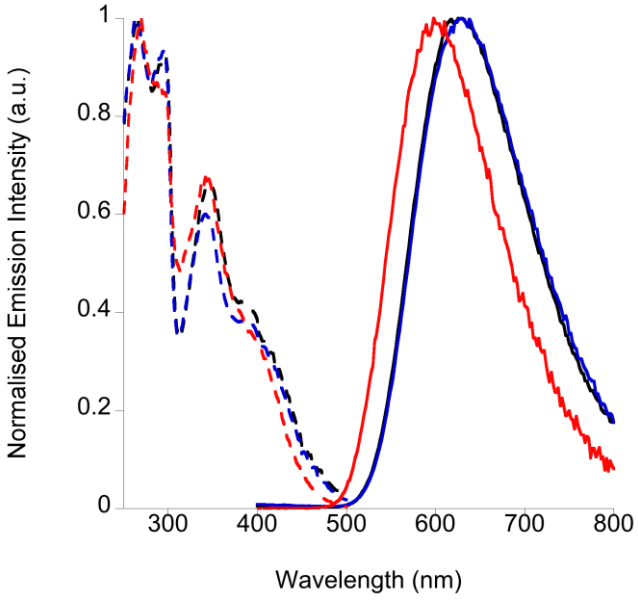

Figure 5. Excitation (dashed lines) and emission profiles (continuous lines) for **S-ReCl** (black trace), **EG-S-ReCl** (blue trace) and **EG-S-ReTPh** (red trace) measured from diluted dichloromethane solutions at room temperature.

The emission profiles of the complexes at 77 K in frozen dichloromethane matrices appear blue-shifted (Figure 6) as a consequence of rigidochromism.[26] The emission profiles appear highly structured and virtually superimposable. The excited state lifetimes reach values of hundreds of μs, which is significantly elongated with respect to previously reported measurements of analogous complexes in frozen matrices. This behaviour seems to indicate that the rigidochromic effect has raised the energy of the emissive ^{3}MLCT/^{3}LLCT excited states above the energy of the ^{3}LC transition involving the S atom.[27] As this ^{3}LC transition does not involve any contribution from the ancillary ligand, the emission is identical irrespectively as to whether the complexes possess a rhenium-chloro or a rhenium-tetrazolato bond.

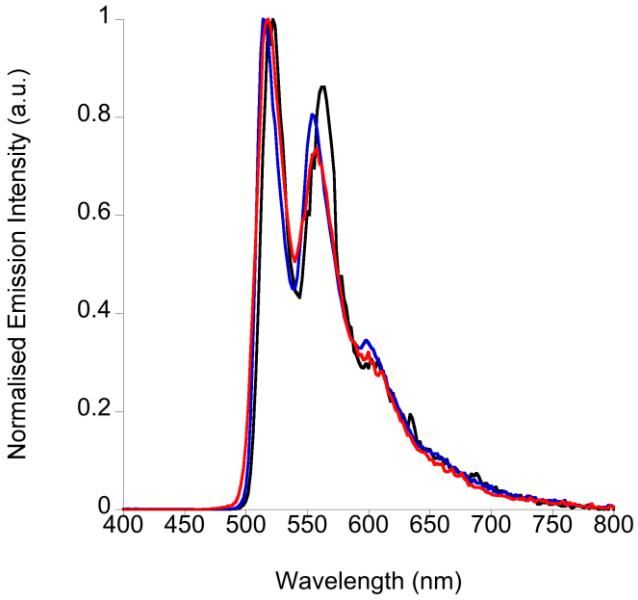

Figure 6. Emission profiles for **S-ReCl** (black trace), **EG-S-ReCl** (blue trace) and **EG-S-ReTPh** (red trace) measured from diluted dichloromethane solutions at 77 K.

Lipophilic character of the complexes

In order to evaluate the potential of the complexes to be incubated in live cells, it is important to know their lipophilic character. The *n*-octanol/water distribution coefficients ($\log D_{7.4}$) of the complexes were measured using the shake-flask method[28] and are summarised in Table 2. The aqueous layer was composed of PBS solution buffered at pH = 7.4. The substitution of the chloro for the tetrazolato ligand increases the lipophilicity of the complexes to values higher than 2. These values are expected as previous work on the incubation of Re tetrazolato complexes within *Drosophila* larval fat body tissue and live human adipose cells suggested passive diffusion through the cellular membrane.[17] The addition of the short ethylene glycol chain does not seem to significantly alter the lipophilicity.

Table 2. Distribution coefficient values for the complexes obtained from 7.4-buffered PBS solutions and *n*-octanol.

Complex	log$D_{7.4}$
ReTPh	2.66 ± 0.11
ReTBz	2.37 ± 0.05
S-ReCl	1.63 ± 0.02
EG-S-ReCl	1.94 ± 0.10
EG-S-ReTPh	2.36 ± 0.07

Incubation in live HeLa cells

All the complexes were incubated in live HeLa cells and their cellular distribution were assessed with the use of confocal microscopy with the excitation source set at 405 nm. Solubilisation in DMSO was required prior to incubation. In all experiments, the final concentration of DMSO in the cell culture was consistently kept below 0.5% (v/v), while the final concentration of the Re complex was maintained around 20 μM. All the presented confocal images were collected after 4 hours incubation to assess whether the complex would show any sign of toxicity while the cells were kept in the dark. The typical Re luminescence, however, could already be detected 30 minutes after incubation. This suggests fast internalisation in an analogous fashion to the previously investigated Re tetrazolato complexes in *Drosophila* larval fat body tissue and live human adipose 3T3-L1 cells.[17] Assessment of the cellular membrane integrity over a four hours period in the dark revealed no signs of toxicity, either for cells incubated with the various complexes or with control cells incubated with only DMSO. Lack of cytotoxicity was crosschecked and confirmed by means of MTS assay.

The composition of the solution containing the Re complex added to the HeLa cells proved to be of critical importance to avoid toxicity issues, even when maintaining the final concentration of the complex at 20 μM. Addition of concentrated solutions of the Re complex in pure DMSO showed signs of localised membrane blebbing at the dropping point. Identical results were obtained by adding the same amount of DMSO but without the Re complex, indicating that toxicity issues were arising from the high local concentration of DMSO (see ESI). Therefore, the DMSO solutions containing the Re complexes were previously diluted in DMEM (Dulbecco's Modified Eagle's

medium) cell medium before addition to the cells. Adding solutions of the Re complex in a DMSO/DMEM mixture did not cause visible membrane blebbing.

Irrespectively of their ligands, all the complexes showed good cellular uptake in live HeLa cells (Figure 7 and see ESI for the remaining complexes) as demonstrated by comparing the differential interference contrast (DIC), luminescence, and merged images. The confocal images highlight internalisation within the cellular membrane and perinuclear cytoplasmic localisation.

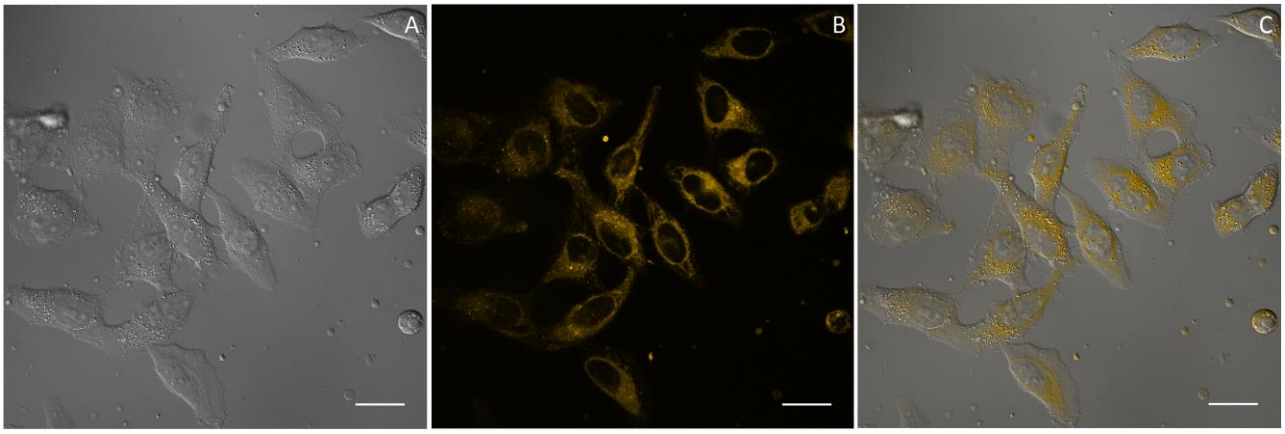

Figure 7. HeLa cells incubated with **ReTPh**. DIC (A) shows the structural integrity of the cells where the luminescence (B) and merged (C) images illustrate cellular uptake and perinuclear localisation of **ReTPh**. Scale bar is 25 μm.

To ensure that the luminescence was originating from the Re complex, rather than cellular autofluorescence, the spectral profile from the perinuclear region of stained cells was compared to the spectral emission of the same region in untreated cells (Figure 8 and see ESI for remaining complexes). The profiles measured from stained cells highlight broad and structureless bands that are analogous to those measured in dichloromethane solutions. On the other hand, spectral profiles from blank cells showed emission of considerably lower intensity without the presence of a broad and structureless band in the 500-750 nm region. Overall, the emission intensities collected from the Re complexes bound to the tetrazolato ligands were higher than those of the chloro-bound complexes. While accurate measurements of the concentration of each Re complex is warranted, this could be tentatively ascribed to the reduced lipophilicity of both **S-ReCl** and **EG-S-ReCl** causing a lower degree of internalisation.

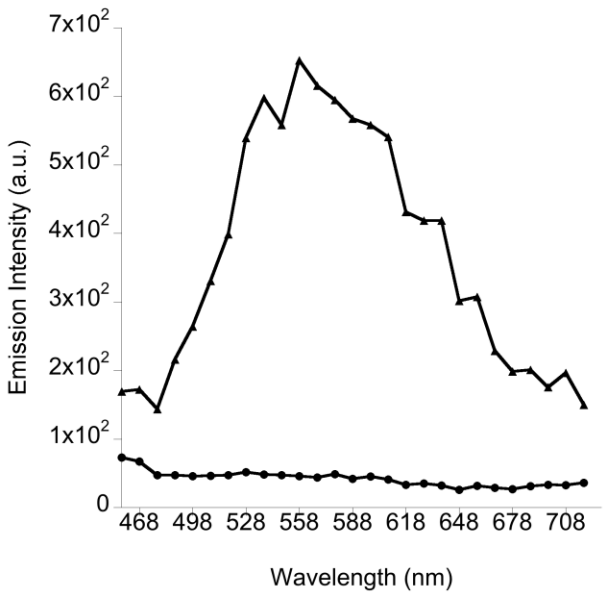

Figure 8. Emission profile from the perinuclear region of live HeLa cells incubated with **ReTPh** (triangles) and from the perinuclear region of untreated live HeLa cells (circles).

The cells could be imaged multiple times with a resting period in the dark of at least 30 seconds between successive scans. No evident sign of photobleaching was detected and the luminescence of the Re complexes was never found to be significantly decreased. The lack of major photobleaching is an important factor indicating that these Re complexes are suitable building blocks for live cell imaging that require multiple excitations over extended time periods. No signs of induced toxicity were detected after multiple imaging for **ReTPh**, **ReTBz**, **S-ReCl**, and **EG-S-ReCl**. However, upon attempting a *z*-scan experiment to identify the 3-dimensional localisation of the Re complexes, the cells showed evident sign of membrane blebbing. Interestingly, the same *z*-scan experiment performed on a blank sample of live HeLa cells incubated with 1% DMSO, but without the Re complex, did not show any sign of blebbing (Figure 9). Therefore, the toxicity was attributed to the possibility that the continuous excitation of the Re complex within the cell might cause an excessive production of $^1O_2$.[6] These results highlight the importance of allowing sufficient time between imaging sessions that require the excitation of triplet state emitters.

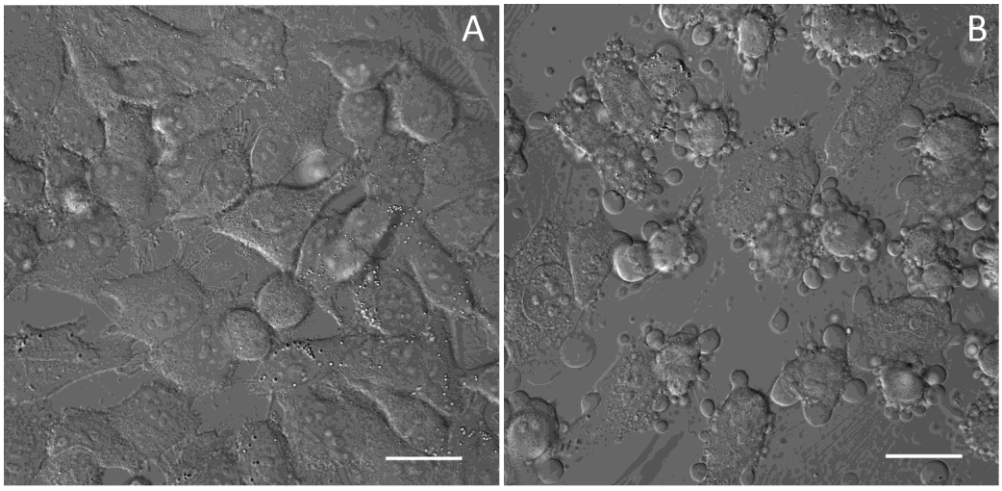

Figure 9. DIC images of HeLa cells after *z*-stack images. HeLa cells incubated with 1% v/v DMSO (A) and HeLa cells incubated with **ReTPh** (B). The control (A) does not show signs of stress however the cells incubated with **ReTPh** (B) have rounded up and show signs of blebbing. Scale bar, 25 μm.

While the behaviour of the **EG-S-ReTPh** complex was analogous to the other complexes in terms of cellular uptake and perinuclear localisation, confocal imaging of live HeLa cells incubated with this complex revealed significantly increased photocytotoxicity (Figure 10). Images taken of cells after 4 hours of incubation in the dark showed an uncompromised cellular membrane, but evident signs of blebbing appeared after multiple images were collected, even if a 30 seconds recovery was allowed after each image. The same imaging modality done in parallel on control (DMSO only) live HeLa cells, where just the same amount of DMSO was added, did not show any sign of membrane blebbing (see ESI). The results point out that the toxicity arises from this particular Re complex and further investigation is underway to determine its origin. Of note, no evident signs of cytotoxicity were evident via MTS test, even when early indication of membrane blebbing was identified via confocal microscopy.

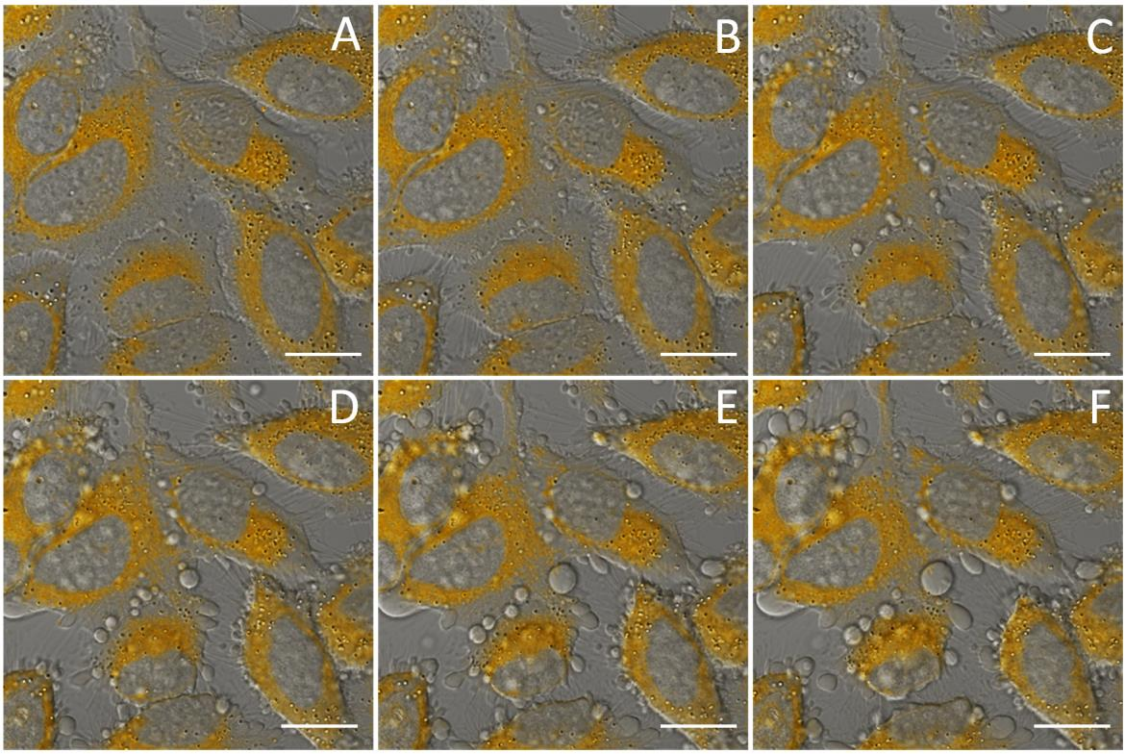

Figure 10. Merged DIC and confocal fluorescence images from a five minute time lapse experiment of HeLa cells incubated with **EG-S-ReTPh.** The combined images were taken at t=0 (A), t=1 min (B), t=2 min (C), t=3 min (D), t=4 min (E) and t=5 min (F). Blebs are apparent at t=2 min (C). Scale bar, 25 μm.

Conclusions

In this work, the cellular incubation of a small family of phosphorescent Re complexes was investigated using live HeLa cells. The Re complexes were varied on the ancillary position between the chloro or tetrazolato ligands and at the diimine between 1,10-phenanthroline and thioalkyl-substituted phenanthroline appended with a short ethylene glycol functionality. Three new complexes were synthesised and photophysically characterised, revealing that the substitution on the phenanthroline ligand does not have an effect on the overall photophysical properties of the complexes at room temperature. These are characterised by emission that is typical of mixed ^{3}MLCT/^{3}LLCT excited states. The only differentiation appears at 77 K, where the emissive state appears predominantly ^{3}LC in nature as the ^{3}MLCT/^{3}LLCT states raise in energy as a consequence of the rigidochromic effect. Overall the complexes in HeLa cells have an analogous behaviour, showing good internalisation and non-specific cytoplasmic localisation. The results highlight important aspects on the specific confocal imaging protocol, as the emissive triplet states of the complexes are able to sensitise singlet oxygen in cells. Excessive production of singlet oxygen, as

in *z*-scan experiments, is clearly detrimental in terms of cytotoxicity. On the other hand, this type of Re complexes does not appear to be toxic while the cells are maintained the dark. The complex **EG-S-ReTPh** shows evidence of acute levels of photocytotoxicity and further investigation is underway to assess its structure-property relationship. The combined results highlight that Re tetrazolato complexes are suitable building blocks for the design of luminescent markers suitable for live cell imaging.

Experimental Section

General Considerations

Unless otherwise stated, all reagents and solvents were purchased from Sigma Aldrich and used as received without further purification. All reactions were conducted under an atmosphere of N_2. 1H-5-phenyltetrazole,[29] **ReTPh**,[12] **ReTBz**,[12] and *fac*-[Re(CO)$_3$(**ephen**)Cl][20] were prepared according to previously published procedures. Nuclear magnetic resonance spectra were recorded using a Bruker Avance 400 spectrometer (400.1 MHz for ^{1}H; 100 MHz for ^{13}C) at 300 K. All the NMR spectra were calibrated to residual solvent signals. Infrared spectra were recorded using an attenuated total reflectance Perkin Elmer Spectrum 100 FT-IR with a diamond stage. IR spectra were recorded from 4000 to 650 cm^{-1}. The intensities of the IR bands are reported as strong (s), medium (m), or weak (w), with broad (br) bands also specified. Melting points were determined using a BI Barnsted Electrothermal 9100 apparatus. Elemental analyses were obtained at Curtin University using a Thermo Finnigan EA 1112 Series Flash.

Synthesis of S-ReCl

fac-[Re(CO)$_3$(**ephen**)Cl] (149 mg, 0.296 mmol) was added to a sodium ethoxide solution in ethanol (0.1 M, 10 mL) followed by 2-mercaptoethanol (0.25 mL, 0.355 mmol). The suspension was allowed to stir at room temperature overnight. After evaporation of the solvent, the crude product was purified via column chromatography on acidic alumina using a dichloromethane/methanol (9.5:0.5) mixture as the eluent (second fraction, yellow). Fraction two was filtered over Celite and reprecipitated from ethyl acetate and petroleum spirits. Yield: 0.076 g, 74%. M.p. 236 °C (dec.). Anal. calcd. for $C_{17}H_{12}N_2ClO_4SRe$: C 36.33, H 2.15, N 4.98, S 5.76; found: C 36.42, H 2.17, N 4.85, S 5.87. ν_{max}/cm^{-1}: 3358 w, 3067 w, 2881 w, 2016 s (CO), 1907 m (CO), 1879 s (CO), 1754 w, 1600 w, 1421 m, 1186 w, 1146 w, 972 w, 874 w, 802 w, 724 w. ^{1}H-NMR δ/ppm (acetone-d$_6$): 9.53 (1H, dd, ^3J = 5.1 Hz, ^4J = 1.3 Hz, **phen** H_9), 9.37 (1H, dd, ^3J = 5.1 Hz, ^4J = 1.3 Hz, **phen** H_2),

9.15 (1H, m, **phen** H_7), 8.81 (1H, m, **phen** H_4), 8.31 (1H, s, **phen** H_5), 8.19 (1H, dd, ^3J = 8.5 Hz, ^4J = 5.1 Hz, **phen** H_8), 8.08 (1H, m, **phen** H_3), 4.28 (1H, s, O*H*), 3.92 (2H, t, ^3J = 6.3 Hz, SCH_2CH_2OH), 3.44 (2H, t, J = 6.3 Hz, SCH_2CH_2OH). ^{13}C-NMR δ/ppm (acetone-d_6): 154.4 (**phen** C_9), 153.3 (**phen** C_2), 147.7 (Ar *C*), 146.3 (Ar *C*), 138.6 (**phen** C_4), 137.3 (Ar *C*), 136.6 (**phen** C_7), 131.7 (Ar *C*), 131.2 (Ar C), 127.5 (**phen** C_3), 127.1 (**phen** C_8), 125.4 (**phen** C_5), 60.8 (SCH_2CH_2OH), 36.7 (SCH_2CH_2OH. Crystals suitable for X-ray analysis were obtained by diffusion of vapours between diethyl ether and a dichloromethane solution of the complex.

Synthesis of EG-S-ReCl

To dry dichloromethane in an ice bath, **S-ReCl** (69 mg, 0.123 mmol), 2-(2-methoxyethoxy)acetic acid (14 μL, 0.123 mmol) and 4-dimethylaminopyridine (4 mg, 0.034 mmol) were combined and stirred at room temperature. After 30 min, 1-ethyl-3-(3-dimethyl-aminopropyl)carbodiimide hydrochloride (25 mg, 0.130 mmol) was added to the reaction. The solution was allowed to warm to room temperature and then stirred for 60 h. The solvent was removed and the product dissolved in ethyl acetate (30 mL). The organic phase was washed with water (10 mL), saturated $NaHCO_3$ solution (3 × 20 mL) and water again (2 × 10 mL). The organic layer was then dried over anhydrous $MgSO_4$. The crude product was purified via column chromatography on acidic alumina using a chloroform/ethyl acetate (8:2) solvent system mixture as the eluent. The complex was collected as the first fraction, which was reprecipitated from ethyl acetate and petroleum spirits. Yield: 0.017 g, 31%. M.p. 143 °C (dec.). Anal. calcd. for $C_{22}H_{20}ClN_2O_7SRe$: C 38.97, H 2.97, N 4.13, S 4.73; found: C 38.81, H 3.02, N 4.02, S 4.64. ν_{max}/cm^{-1}: 3285 w, 2892 w, 2016 s (CO), 1886 s (CO), 1755 m, 1600 w, 1421 m, 1185 w, 1144 w, 1113 w, 971 w, 883 w, 803 w, 726 w. ^{1}H-NMR δ/ppm (acetone-d_6): 9.54 (1H, dd, ^3J = 5.1 Hz, ^4J = 1.3 Hz, **phen** H_9), 9.41 (1H, dd, ^3J = 5.1 Hz, ^4J = 1.3 Hz, **phen** H_2), 9.18 (1H, dd, ^3J = 8.4 Hz, ^4J = 1.3 Hz, **phen** H_7), 8.82 (1H, dd, ^3J = 8.4 Hz, ^4J = 1.3 Hz, **phen** H_4), 8.44 (1H, s, **phen** H_5), 8.21 (1H, dd, ^3J = 8.4 Hz, ^4J = 5.1 Hz, **phen** H_8), 8.10 (1H, dd, ^3J = 8.4 Hz, ^4J = 5.1 Hz, **phen** H_3), 4.49 (2H, t, J = 6.4 Hz, SCH_2CH_2O), 4.06 (2H, s, $OCOCH_2O$), 3.61 (2H, t, ^3J = 6.4 Hz, SCH_2CH_2O), 3.59 (2H, m, $OCH_2CH_2OCH_3$), 3.45 (2H, m, $OCH_2CH_2OCH_3$), 3.26 (3H, s, OCH_3). ^{13}C-NMR δ/ppm (acetone-d_6): 198.8 (*C*O), 190.7 (*C*O), 170.9 (O*C*O(CH_2)), 154.4 (**phen** C_9), 153.7 (**phen** C_2), 147.9 (Ar *C*), 146.6 (Ar *C*), 138.8 (**phen** C_4), 136.8 (**phen** C_7), 135.9 (Ar *C*), 131.5 (Ar *C*), 131.3 (Ar C), 127.6 (**phen** C_3), 127.3 (**phen** C_8), 127.2 (**phen** C_5), 72.6 ($OCH_2CH_2OCH_3$), 71.3 (SCH_2CH_2O), 68.8 ($OCO(CH_2)$), 63.0 (SCH_2CH_2O), 58.8 (OCH_3), 32.8 ($OCH_2CH_2OCH_3$). Crystals suitable for X-ray analysis were obtained by diffusion of vapours between petroleum spirits and a dichloromethane solution of the complex.

Synthesis of EG-S-ReTPh

Silver triflate (26 mg, 0.10 mmol) and **EG-S-ReCl** (47 mg, 0.07 mmol) were combined in chloroform (10 mL) and heated at reflux for 20 h in the dark. The solution was filtered over Celite and 5-phenyl-1H-tetrazole (15 mg, 0.10 mmol) and triethylamine (14 μL, 0.10 mmol) were added to the solution, which was then heated at reflux for 48 h. The solvent was evaporated, and the resulting residue was purified via column chromatography on acidic alumina using acetonitrile as the eluent (second fraction, yellow). The residue obtained from the drying of this fraction was dissolved in dichloromethane (*ca* 1 mL) and filtered through a plug of Celite into stirring pentane. The resulting yellow solid was collected, washed with pentane (3 × 3 mL), and air-dried. Yield: 0.009 g, 17%. Repeated attempts at obtaining an elemental composition within ± 0.5% were unsuccessful due to the low yields obtained and the difficulty of purification. Anal. calcd. for $C_{29}H_{25}N_6O_7SRe_{\bullet}(0.5CH_2Cl_2)$: C 42.67, H 3.16, N 10.12, S 3.86; found: C 42.17, H 2.12, N 11.52, S 3.39. ν_{max}/cm^{-1}: 2929 w, 2025 s (CO), 1908 (CO), 1752 w, 1609 w, 1599 w, 1425 w, 1199 w. ^{1}H-NMR δ/ppm (acetone-d_6): 9.70 (1H, dd, ^3J = 5.2 Hz, ^4J = 1.3 Hz, **phen** H_9), 9.55 (1H, dd, ^3J = 5.1 Hz, ^4J = 1.4 Hz, **phen** H_2), 9.16 (1H, dd, ^3J = 8.5 Hz, ^4J = 1.3 Hz, **phen** H_7), 8.79 (1H, dd, ^3J = 8.4 Hz, ^4J = 1.4 Hz, **phen** H_4), 8.37 (1H, s, **phen** H_5), 8.21 (1H, dd, ^3J = 8.5 Hz, ^4J = 5.1 Hz, **phen** H_8), 8.10 (1H, dd, ^3J = 8.4 Hz, ^4J = 5.1 Hz, **phen** H_3), 7.67 (2H, dd, ^3J = 8.2 Hz, ^4J = 1.6 Hz, CN_4-C_6H_5 H_{ortho}), 7.18−7.27 (3H, 2 × m, CN_4-C_6H_5 H_{meta} and H_{para}), 4.45 (2H, t, J = 6.4 Hz, SCH_2CH_2O), 4.06 (2H, s, $OCOCH_2O$), 3.59 (2H, t, ^3J = 6.4 Hz, SCH_2CH_2O), 3.56 (2H, m, $OCH_2CH_2OCH_3$), 3.45 (2H, m, $OCH_2CH_2OCH_3$), 3.26 (3H, s, OCH_3). ^{13}C-NMR δ/ppm (acetone-d_6): 197.9 (*C*O), 194.8 (*C*O), 170.9 (O*C*O(CH_2)), 163.7 (*C*N_4-C_6H_5), 155.4 (**phen** C_9), 154.5 (**phen** C_2), 148.6 (Ar *C*), 147.3 (Ar *C*), 139.2 (**phen** C_4), 137.1 (**phen** C_7), 136.0 (Ar *C*), 131.3 (Ar *C*), 131.2 (Ar *C*), 131.0 (**phen** C_{11}), 129.1 (phenyl C_{meta}), 128.9 (phenyl C_{para}), 127.8 (**phen** C_3), 127.4 (**phen** C_8), 126.8 (**phen** C_5), 126.7 (phenyl C_{ortho}), 72.6 ($OCH_2CH_2OCH_3$), 71.3 (SCH_2CH_2O), 68.8 (OCO(CH_2), 62.9 (SCH_2CH_2O), 58.8 (OCH_3), 32.7 ($OCH_2CH_2OCH_3$).

X-ray diffraction analysis

Crystallographic data for the structures were collected at 100(2) K on an Oxford Diffraction Xcalibur **(S-ReCl)** fitted with Mo Kα radiation (λ = 0.71073 Å) or a Gemini **(EG-S-ReCl)** diffractometer fitted with Cu Kα radiation (λ = 1.54178 Å). Following analytical absorption corrections and solution by direct methods, the structures were refined against F^2 with full-matrix least-squares using the program SHELXL-97.[30] Anisotropic displacement parameters were employed for the non-hydrogen atoms. All hydrogen atoms were added at calculated positions and

refined by use of a riding model with isotropic displacement parameters based on those of the parent atom.

Crystal data

S-ReCl. Formula: $C_{18}H_{14}Cl_3N_2O_4ReS$, M = 646.92. Monoclinic, space group $P2_1/c$, a = 10.1763(5), b = 20.8369(4), c = 10.3782(3) Å, β= 110.147(4)°, V = 2065.97(12) Å^3, Z = 4, D_{calc} = 2.080 Mg m^{-3}, μ = 6.399 mm^{-1}, $2\theta_{max}$ = 66°, crystal size = 0.15 x 0.06 x 0.05 mm^3. Reflections collected = 56790, unique = 7775, R_{int} = 0.0525. Data / restraints / parameters = 7775 / 3 / 279, GooF = 1.110. Final R indices (I>2σ(I)): R_1 = 0.0383, wR_2 = 0.0679. R indices (all data): R_1 = 0.0497, wR_2 = 0.0710. $\Delta\rho_{max,min}$ = 1.743, -1.625 e. Å^{-3}. CCDC 1419756. The dichloromethane solvent molecule was modelled as being disordered over two sets of sites with occupancies refined to 0.907(2) and its complement. The geometries of the minor component were restrained to ideal values.

EG-S-ReCl. Formula: $C_{22}H_{20}ClN_2O_7ReS$, M = 678.11. Triclinic, space group $P\bar{1}$. a = 11.5291(11), b = 13.1863(12), c = 16.323(2) Å , α= 90.450(8), β= 92.944(8), γ = 110.770(9)°, V = 2316.3(4) Å^3, Z = 4, D_{calc} = 1.945 Mg m^{-3}, μ = 12.585 mm^{-1}, $2\theta_{max}$ = 134.72°, crystal size = 0.25 x 0.05 x 0.015 mm^3. Reflections collected = 23868, unique = 8213, R_{int} = 0.0464. Data / restraints / parameters = 8213 / 0 / 615, GooF = 1.044. Final R indices (I>2σ(I)): R_1 = 0.0466, wR_2 = 0.1131. R indices (all data): R_1 = 0.0569, wR_2 = 0.1229. $\Delta\rho_{max,min}$ = 3.640 and -0.944 e.Å^{-3}. CCDC 1419757.

Photophysical measurements

Absorption spectra were recorded at room temperature using a Cary 4000 UV/Vis spectrometer. Uncorrected steady state emission and excitation spectra were recorded on an Edinburgh FLSP980-S2S2-stm spectrometer equipped with: i) a temperature-monitored cuvette holder; ii) 450 W Xenon arc lamp; iii) double excitation and emission monochromators; iv) a Peltier cooled Hamamatsu R928P photomultiplier tube (spectral range 200-870 nm) or a Hamamatsu R5509-42 photomultiplier for detection of NIR radiation (spectra range 800-1400 nm). Emission and excitation spectra were corrected for source intensity (lamp and grating) and emission spectral response (detector and grating) by a calibration curve supplied with the instrument. To record the 77 K luminescence spectra and emission lifetimes, the samples were put in glass tubes (2 mm diameter) and inserted in a special quartz Dewar filled up with liquid nitrogen. According to the approach described by Demas and Crosby,[31] luminescence quantum yields (Φ_{em}) were measured in

optically dilute solutions (O.D. < 0.1 at excitation wavelength) obtained from absorption spectra on a wavelength scale [nm] and compared to the reference emitter by the following equation:

$$\Phi_x = \Phi_r \frac{A_r(\lambda_r)}{A_x(\lambda_x)} \frac{I_r(\lambda_r)}{I_x(\lambda_x)} \frac{n_x^2}{n_r^2} \frac{D_x}{D_r}$$

where A is the absorbance at the excitation wavelength (λ), I is the intensity of the excitation light at the excitation wavelength (λ), n is the refractive index of the solvent, D is the integrated intensity of the luminescence and Φ is the quantum yield. The subscripts r and x refer to the reference and the sample, respectively. The quantum yield determinations were performed at identical excitation wavelength for the sample and the reference, therefore cancelling the $I(\lambda_r)/I(\lambda_x)$ term in the equation. The quantum yields of complexes were measured against an air-equilibrated 0.1 M H_2SO_4 solution of quinine sulfate (Φ_r = 0.53).[32] Emission lifetimes (τ) were determined with the time correlated single photon counting technique (TCSPC) with the same Edinburgh FLSP980-S2S2-stm spectrometer using either a pulsed picosecond LED (EPLED/EPL 377 nm, FHWM < 800 ps) or a microsecond flashlamp The goodness of fit was assessed by minimising the reduced χ^2 function and by visual inspection of the weighted residuals. The solvents used for the preparation of the solutions for the photophysical investigations were of LR grade and the water was deionised. Experimental uncertainties are estimated to be ±8% for lifetime determinations, ±20% for quantum yields, ±2 nm and ±5 nm for absorption and emission peaks, respectively.

TDDFT Calculations

Time-dependent density functional theory calculations were performed with GAUSSIAN 09.[33] Prior to these calculations, the structures were relaxed at the CAM-B3LYP level of theory. The Re atoms were treated with the Stuttgart-Dresden effective core potential,[34] the Pople 6-311G** basis set was used for C, H, N, O, Cl, and S atoms, and the effect of the solvent was mimicked with the PCM solvation model,[24] with parameters adequate for dichloromethane. The low-lying singlet−singlet excitation energies were calculated at the same level of theory, and the spectra were reproduced as the superposition of Gaussian functions with heights proportional to calculated intensities and a variance of 11 nm. Comparisons of crystal structures to minimised geometry were calculated utilizing the RMSD analysis tool in VMD and neglecting the ethylene glycol chains and protons.

Cellular cultures

Human cervical carcinoma cells (HeLa) were cultured in DMEM cell medium (Gibco, Australia), 10% Fetal Bovine Serum (Gibco, Australia), and 1% penicillin-streptomycin at 37 °C under a 5% CO_2 atmosphere in T75 culture flasks. When the cells were ready for imaging, they were treated with 1 mL of trypsin (0.1%) and seeded into 35 mm diameter Mattek glass coverslip bottom petri dishes for 24 hours before imaging, in order to give a cell confluency of 50-60%. DMSO solutions of the prepared complexes were added to 2 mL of culture media and then added to the cell cultures to give final concentrations of the complexes between 10-20 μM. The DMSO concentration for each experiment was kept within the 0.4-0.5% range in the culture media.

Determination of lipophilicity

The *n*-octanol/water distribution coefficient of the complexes was determined by the shake-flask method.[28] PBS buffer (pH 7.4) and *n*-octanol were mixed together over 72 hours to ensure saturation of both phases. Each complex (1 mg) was dissolved in 250 μL of DMSO. To a 1:1 solvent system of PBS buffer and *n*-octanol (750 μL each), 50 μL of the complex in DMSO was added and mixed using a laboratory vortexer. The resulting solution was centrifuged (3000 RCF, 5 min) to allow separation of the two phases and removal of any emulsions. The absorption profile of the complex in each phase was measured by UV-Vis spectroscopy ensuring that any necessary dilution was carried out to keep the absorbance below 1. The absorbance at 280 nm was recorded and used to determine the log *D* value where:

$$\log D = \log A_o - \log A_w$$

where A_o and A_w are the absorbance values of the complex in the *n*-octanol and water phases measured at λ = 280 nm, respectively. The method assumed constant molar absorptivity between the two solvents so that, according to Beer's law, the values of concentration are linearly proportional to the values of absorbance.

Confocal imaging

All confocal imaging and spectral detection experiments were carried out on a Nikon A1Si confocal microscope. Köhler alignment was carried out before each imaging session and differential interference contrast (DIC) imaging was always employed. The Nikon A1Si confocal microscope system was equipped with four PMT detectors, 32 channel spectral detector and 50mW solid state

lasers of the following wavelengths: 405 nm, 488 nm, 561 nm and 638 nm. The 405 nm laser was used for excitation and the images were collected in channels 2, 3 and 4 with spectral ranges of 500-550 nm, 570-620 nm and 633-738 nm respectively. For live cell imaging experiments, a Tokai Hit stage top incubation system was used. Images were collected using a Nikon PlanApo 60× VC oil immersion objective with a numerical aperture of 1.4. In cases where spectral detection was carried out, 32-channel spectral images were collected using a 10 nm resolution Si grating and the 405 nm laser for excitation. Images were collected at a resolution of 0.21 μm/pixel (1024×1024 pixels) or 0.41 μm/pixel (512×512 pixels). Confocal images were exported from the Nikon software NIS-Elements as 16 bit mono-color images. FIJI (ImageJ) was used to add the channels 2, 3 and 4 together. The combined image was imported into Photoshop and converted to an RGB image. Color was added by altering the relative values of each RGB channel. Each fluorescence image was processed using the same brightness/contrast and RGB values for consistency. The DIC image was also imported into Photoshop and the two images were overlaid. The fluorescent layer, placed on top, was converted to color using the blending options, which gave the final merged image. The final images were converted to 8 bit and saved as TIFF files.

Acknowledgments

The work was financially supported by the Australian Research Council (FT1301000033 and LE1301000054). MVW wishes to thank Curtin University for the APA scholarship. The authors acknowledge the facilities, and the scientific and technical assistance of the Australian Microscopy & Microanalysis Research Facility at the Centre for Microscopy, Characterisation & Analysis, The University of Western Australia, a facility funded by the University, State and Commonwealth Governments.

References

1 M. P. Coogan and V. Fernández-Moreira, *Chem. Commun.*, 2013, **50**, 384–399.
2 K. Lo, *Top. Organomet. Chem.*, 2010, **29**, 115–158.
3 D. Parker, *Aust. J. Chem.*, 2011, **64**, 239–243.
4 J. A. Thomas, *Chem. Soc. Rev.*, 2015, **44**, 4494–4500.
5 R. G. Balasingham, M. P. Coogan and F. L. Thorp-Greenwood, *Dalton Trans.*, 2011, **40**, 11663–11674.
6 P. Ogilby, *Chem. Soc. Rev.*, 2010, **39**, 3181–3209.
7 S. P. Foxon, M. A. H. Alamiry, M. G. Walker, A. J. H. M. Meijer, I. V. Sazanovich, J. A. Weinstein and J. A. Thomas, *J. Phys. Chem. A*, 2009, **113**, 12754–12762.
8 J. Celli, B. Spring, I. Rizvi, C. Evans, K. Samkoe, S. Verma, B. Pogue and T. Hasan, *Chem. Rev.*, 2010, **110**, 2795–2838.
9 U. Schatzschneider, *Eur. J. Inorg. Chem.*, 2010, 1451–1467.
10 S. S. Kelkar and T. M. Reineke, *Bioconjugate Chem*, 2011, **22**, 1879–1903.

11 L. He, C.-P. Tan, R.-R. Ye, Y.-Z. Zhao, Y.-H. Liu, Q. Zhao, L.-N. Ji and Z.-W. Mao, *Angew. Chem. Int. Ed.*, 2014, **53**, 12137–12141.
12 M. V. Werrett, D. Chartrand, J. D. Gale, G. S. Hanan, J. G. MacLellan, M. Massi, S. Muzzioli, P. Raiteri, B. W. Skelton, M. Silberstein and S. Stagni, *Inorg. Chem.*, 2011, **50**, 1229–1241.
13 P. J. Wright, S. Muzzioli, M. V. Werrett, P. Raiteri, B. W. Skelton, D. S. Silvester, S. Stagni and M. Massi, *Organometallics*, 2012, **31**, 7566–7578.
14 M. V. Werrett, S. Muzzioli, P. J. Wright, A. Palazzi, P. Raiteri, S. Zacchini, M. Massi and S. Stagni, *Inorg. Chem.*, 2014, **53**, 229–243.
15 M. V. Werrett, G. S. Huff, S. Muzzioli, V. Fiorini, S. Zacchini, B. W. Skelton, A. Maggiore, J. M. Malicka, M. Cocchi, K. C. Gordon, S. Stagni and M. Massi, *Dalton Trans.*, 2015, **44**, 8379–8393.
16 S. Stagni, S. Colella, A. Palazzi, G. Valenti, S. Zacchini, F. Paolucci, M. Marcaccio, R. Q. Albuquerque and L. De Cola, *Inorg. Chem.*, 2008, **47**, 10509–10521.
17 C. A. Bader, R. D. Brooks, Y. S. Ng, A. Sorvina, M. V. Werrett, P. J. Wright, A. G. Anwer, D. A. Brooks, S. Stagni, S. Muzzioli, M. Silberstein, B. W. Skelton, E. M. Goldys, S. E. Plush, T. Shandala and M. Massi, *RSC Adv.*, 2014, **4**, 16345–16351.
18 A. W.-T. Choi, M.-W. Louie, S. P.-Y. Li, H.-W. Liu, B. T.-N. Chan, T. C.-Y. Lam, A. C.-C. Lin, S.-H. Cheng and K. K.-W. Lo, *Inorg. Chem.*, 2012, **51**, 13289–13302.
19 M. Joralemon, S. McRae and T. Emrick, *Chem. Commun.*, 2010, **46**, 1377–1393.
20 A. A. Mart, G. Mezei, L. Maldonado, G. Paralitici, R. G. Raptis and J. L. Colón, *Eur. J. Inorg. Chem.*, 2005, 118–124.
21 E. Hevia, J. Pérez, V. Riera, D. Miguel, S. Kassel and A. Rheingold, *Inorg. Chem.*, 2002, **41**, 4673–4679.
22 L. Cuesta, M. A. Huertos, D. Morales, J. Pérez, L. Riera, V. Riera, D. Miguel, A. Menéndez-Velázquez and S. García-Granda, *Inorg. Chem.*, 2007, **46**, 2836–2845.
23 R. A. Kirgan, B. P. Sullivan and D. P. Rillema, *Top. Curr. Chem.*, 2007, **281**, 45–100.
24 J. Tomasi, B. Mennucci and R. Cammi, *Chem. Rev.*, 2005, **105**, 2999–3094.
25 E. Kober, J. Caspar, R. Lumpkin and T. Meyer, *J. Phys. Chem.*, 1986, **90**, 3722–3734.
26 J. R. Lakowicz, *Principles of fluorescence spectroscopy*, Springer, Baltimore, Third Ed., 2009.
27 W. Xue, M. Chan, Z. Su, K. Cheung, S. Liu and C. Che, *Organometallics*, 1998, **17**, 1622–1630.
28 P. C. Kunz, W. Huber, A. Rojas, U. Schatzschneider and B. Spingler, *Eur. J. Inorg. Chem.*, 2009, 5358–5366.
29 K. Koguro, T. Oga, S. Mitsui and R. Orita, *Synthesis*, 1998, 910–914.
30 G. M. Sheldrick, *Acta Cryst. A*, 2008, **64**, 112–122.
31 J. Demas and G. Crosby, *J. Phys. Chem.*, 1971, **75**, 991–1024.
32 D. Eaton, *Pure Appl. Chem.*, 1988, **60**, 1107–1114.
33 M. J. Frisch, G. W. Trucks, H. B. Schlegel, G. E. Scuseria, M. A. Robb, J. R. Cheeseman, G. Scalmani, V. Barone, B. Mennucci, G. A. Petersson, H. Nakatsuji, M. Caricato, X. Li, H. P. Hratchian, A. F. Izmaylov, J. Bloino, G. Zheng, J. L. Sonnenberg, M. Hada, M. Ehara, K. Toyota, R. Fukuda, J. Hasegawa, M. Ishida, T. Nakajima, Y. Honda, O. Kitao, H. Nakai, T. Vreven, J. A. Montgomery, Jr, J. E. Peralta, F. Ogliaro, M. Bearpark, J. J. Heyd, E. Brothers, K. N. Kudin, V. N. Staroverov, R. Kobayashi, J. Normand, K. Raghavachari, A. Rendell, J. C. Burant, S. S. Iyengar, J. Tomasi, M. Cossi, N. Rega, J. M. Millam, M. Klene, J. E. Knox, J. B. Cross, V. Bakken, C. Adamo, J. Jaramillo, R. Gomperts, R. E. Stratmann, O. Yazyev, A. J. Austin, R. Cammi, C. Pomelli, J. W. Ochterski, R. L. Martin, K. Morokuma, V. G. Zakrzewski, G. A. Voth, P. Salvador, J. J. Dannenberg, S. Dapprich, A. D. Daniels, Ö. Farkas, J. B. Foresman, J. V. Ortiz, J. Cioslowski and D. J. Fox, *Gaussian09, Revision B.01*, Wallingford, CT.
34 D. Andrae, U. Haeussermann, M. Dolg, H. Stoll and H. Preuss, *Theor. Chim. Acta*, 1990, **77**,

123–141.